Tsunamis

Steven N. Ward
Institute of Tectonics, University of California at Santa Cruz

GLOSSARY

dispersive: *Characteristic of waves whose velocity of propagation depends on wave frequency. The shape of a dispersive wave packet changes as it moves along.*

eigenfunction: *Functional shape of the horizontal and vertical components of wave motion versus depth in the ocean for a specific wave frequency.*

geometrical spreading: *Process of amplitude reduction resulting from the progressive expansion of a wave from its source.*

shoal: *Process of waves coming ashore. Shoaling waves slow, shorten their wavelength, and grow in height.*

wavenumber: *Wavenumber* k *equals* 2π *divided by wavelength* λ. *Large wavenumbers associate with short waves and small wavenumbers associate with long waves.*

Tsunamis are gravity waves that propagate near the ocean surface. Tsunamis belong to the same family as common sea waves that we enjoy at the beach; however, tsunamis are distinct in their mode of generation and in their characteristic period, wavelength, and velocity. Unlike common sea waves that evolve from persistent surface winds, most tsunamis spring from sudden shifts of the ocean floor. These sudden shifts can originate from undersea landslides and volcanoes, but mostly, submarine earthquakes parent tsunamis. Reflecting this heritage, tsunamis often are called seismic sea waves. Compared with wind-driven waves, seismic sea waves have periods, wavelengths, and velocities ten or a hundred times larger. Tsunamis thus have profoundly different propagation characteristics and shoreline consequences than do their common cousins.

I. Tsunami = Killer Wave?

Perhaps influenced by Hollywood movies, some people equate tsunamis with killer waves. Certainly a five-meter high tsunami born from a great earthquake is impressive. So too is the fact that a tsunami can propagate thousands of kilometers and still pack a punch. Upon reaching shore, tsunami waves ***shoal*** and become more menacing still. Understandably, the most damaging cases of natural hazards come to mind, but it is important to keep perspective. Tsunamis over a meter or two in height are not common. A submarine earthquake greater than magnitude M8 must happen to make a wave of this size. On a global average, about one M8+ earthquake occurs per year. Of these, maybe 1-in-10 strikes

under the ocean with a fault orientation favorable for tsunami excitation. Thus, tsunamis that induce widespread damage number about one or two per decade. Although one's concepts might be cast by rare "killer tsunamis", many more benign ones get lost in the shuffle. Today, ocean bottom pressure sensors can detect a tsunami of a few centimeters height even in the open sea. Because numerous, moderate (≈M6.5) earthquakes can bear waves of this size, "baby" tsunamis occur several times per year. They pass by generally unnoticed, except by scientists. Perhaps while swimming in the surf, the reader has already been in a tsunami! Whether killer waves or ripples, tsunamis span three phases: generation, propagation and shoaling. This article touches gently on each.

II. Characteristics of Tsunamis

A. Tsunami Velocity, Wavelength, and Period

This article reviews classical tsunami theory. Classical theory envisions a rigid seafloor overlain by an incompressible, homogeneous, and non-viscous ocean subjected to a constant gravitational field. Classical tsunami theory has been investigated widely, and most of its predictions change only slightly under relaxation of these assumptions. This article draws upon linear theory that also presumes that the ratio of wave amplitude to wavelength is much less than one. By and large, linearity is violated only during the final stage of wave breaking and perhaps, under extreme nucleation conditions.

In classical theory, the phase $c(\omega)$, and group $u(\omega)$ velocity of surface gravity waves on a flat ocean of uniform depth h are

$$c(\omega) = \sqrt{\frac{gh\ \tanh[k(\omega)h]}{k(\omega)h}} \quad (1)$$

and

$$u(\omega) = c(\omega)\left[\frac{1}{2} + \frac{k(\omega)h}{\sinh[2k(\omega)h]}\right] \quad (2)$$

Here, g is the acceleration of gravity (9.8 m/s^2) and $k(\omega)$ is the ***wavenumber*** associated with a sea wave of frequency ω. Wavenumber connects to wavelength $\lambda(\omega)$ as $\lambda(\omega)=2\pi/k(\omega)$. Wavenumber also satisfies the relation

$$\omega^2 = gk(\omega)\tanh[k(\omega)h] \quad (3)$$

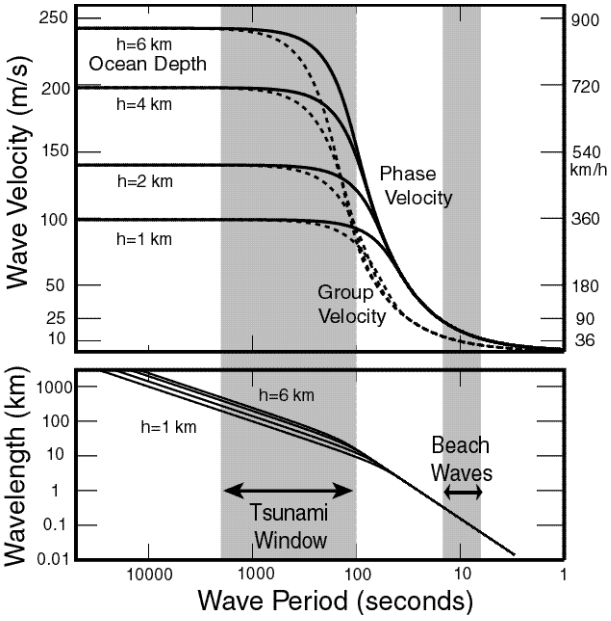

Figure 1. (*top panel*) Phase velocity $c(\omega)$ (solid lines) and group velocity $u(\omega)$ (dashed lines) of tsunami waves on a flat earth covered by oceans of 1, 2, 4 and 6 km depth. (*bottom panel*) Wavelength associated with each wave period. The 'tsunami window' is marked.

For surface gravity waves spanning 1 to 50,000s period, Fig. 1 plots c(ω), u(ω), and λ(ω). These quantities vary widely, both as a function of ocean depth and wave period. Waves whose velocity or wavelength varies with frequency are called ***dispersive***. During propagation, dispersion "pulls apart" originally pulse-like waves into their component frequencies. I emphasize below dispersion's strong influence on attenuating tsunamis.

Common waves at the beach have periods near 10s and wavelengths around 100m (see Fig. 1). Tsunamis on the other hand, because they are generated by seafloor shifts, must have wavelengths greater than three times the ocean depth at the point of their origination. (I explain later why this is so.) This fact fixes a short wavelength bound on tsunamis near 10km. The dimension of the sea floor disturbance itself fixes the upper wavelength bound. The greatest earthquakes might deform a region 500km across. The left gray band of Fig. 1 colors the "tsunami window" (λ=10 to 500km) that spans 100 to 2000s period. Waves in the tsunami window travel rapidly, reaching speeds of 160 to 250m/s (600-900km/hr) in the open ocean – about the speed of a commercial jet airliner. Waves at the beach travel at 10m/s (40km/hr) – about the speed of a moped. The long period, great wavelength, and high velocity of tsunamis help account for their destructive power.

Discussions of waves of length λ in oceans of depth h sometimes include two simplifications: a long wave approximation (λ>>h, 1/k>>h) and a short wave approximation (λ<<h, 1/k<<h). Under a long wave approximation, $kh \to 0$ and equations (1) to (3) predict non-dispersive wave propagation with $c(\omega) = u(\omega) = \sqrt{gh}$. Long wave theory holds for the flat part of the curves in Fig 1. Under a short wave approximation, $kh \to \infty$ and the equations predict dispersive propagation with $c(\omega) = 2u(\omega) = \sqrt{g\lambda(\omega)/2\pi}$. Short wave theory holds to the right in Fig. 1 where all the curves lie atop each other. Waves in the tsunami window have intermediate character, behaving like shallow water waves at their longest periods and like deep-water waves at their shortest periods. Neither the long or short wave simplification serves adequately in tsunami studies. A rigorous treatment requires an approach that works for waves of all lengths.

B. Tsunami Eigenfunctions

Many properties of tsunamis can be understood by examining their ***eigenfunctions***. An eigenfunction describes the distribution of motion in a tsunami mode of a particular frequency. Consider coordinate system (x, y, z) where $\hat{\mathbf{x}}$ points north, $\hat{\mathbf{y}}$ east, and $\hat{\mathbf{z}}$ down. Vertical (u_z) and horizontal (u_x) components of tsunami eigenfunctions normalized to unit vertical displacement at the sea surface are

$$u_z(\omega,z) = \frac{k(\omega)g}{\omega^2} \frac{\sinh[k(\omega)(h-z)]}{\cosh[k(\omega)h]} e^{i[k(\omega)x-\omega t]}$$

$$u_x(\omega,z) = \frac{-ik(\omega)g}{\omega^2} \frac{\cosh[k(\omega)(h-z)]}{\cosh[k(\omega)h]} e^{i[k(\omega)x-\omega t]} \quad (4)$$

Fig. 2 plots tsunami eigenfunctions versus depth in a 4km deep ocean at long (1500s), intermediate (150s) and short (50s) periods. The little el-

lipses can be thought of as tracing the path of a water particle as a wave of frequency ω passes. At 1500s period (left, Fig. 2), the tsunami has a wavelength of λ=297km and it acts like a long wave. The vertical displacement peaks at the ocean surface and drops to zero at the seafloor. The horizontal displacement is constant through the ocean column and exceeds the vertical component by more than a factor of ten. Every meter of visible vertical motion in a tsunami of this

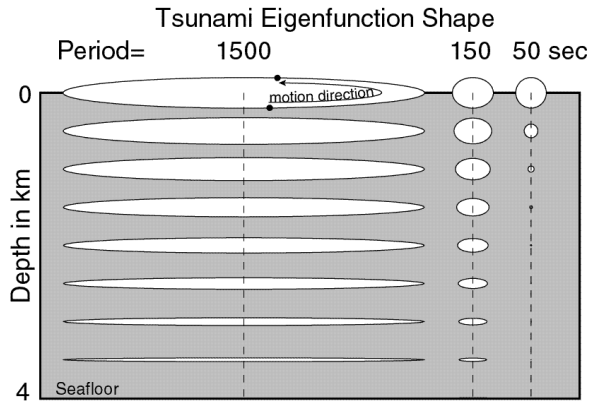

Figure 2. Tsunami eigenfunctions in a 4 km deep ocean at periods 1500, 150 and 50s. Vertical displacements at the ocean surface has been normalized to 1 m in each case.

frequency involves ≈10m of "invisible" horizontal motion. Because the eigenfunctions of long waves reach to the seafloor, the velocity of long waves are sensitive to ocean depth (see top left-hand side of Fig. 1). As the wave period slips to 150s (middle Fig. 2), λ decreases to 26km -- a length comparable to the ocean depth. Long wave characteristics begin to break down, and horizontal and vertical motions more closely agree in amplitude. At 50s period (right, Fig. 2) the waves completely transition to deep water behavior. Water particles move in circles that decay exponentially from the surface. The eigenfunctions of short waves do not reach to the seafloor, so the velocities of short waves are independent of ocean depth (see right hand side of Fig. 1, top). The failure of short waves (λ<<h) to "feel" the seafloor also means that they can not be excited by deformations of it. This is the physical basis for the short wavelength bound on the tsunami window that I mentioned above.

III. Excitation of Tsunamis

Suppose that the seafloor at points $\mathbf{r}_0$ uplifts instantaneously by an amount $u_z^{bot}(\mathbf{r}_0)$ at time $\tau(\mathbf{r}_0)$. Under classical tsunami theory in a uniform ocean of depth h, this sea bottom disturbance produces surface tsunami waveforms (vertical component) at observation point $\mathbf{r}=x\hat{\mathbf{x}}+y\hat{\mathbf{y}}$ and time t of

$$u_z^{surf}(\mathbf{r},t) = \mathrm{Re}\int_{\mathbf{k}} d\mathbf{k}\,\frac{e^{i[\mathbf{k}\cdot\mathbf{r}-\omega(k)t]}}{4\pi^2\cosh(kh)}\,F(\mathbf{k})$$

with (5a,b)

$$F(\mathbf{k}) = \int_{\mathbf{r}_0} d\mathbf{r}_0\; u_z^{bot}(\mathbf{r}_0)\,e^{-i[\mathbf{k}\cdot\mathbf{r}_0-\omega(k)\tau(\mathbf{r}_0)]}$$

with $k=|\mathbf{k}|$, and $\omega^2(k) = gk\tanh(kh)$. The integrals in (5) cover all wavenumber space and locations $\mathbf{r}_0$ where the seafloor disturbance $u_z^{bot}(\mathbf{r}_0)\neq 0$.

Equation (5a) looks scary but it has three identifiable pieces:

a) The $F(\mathbf{k})$ term is the wavenumber spectrum of the seafloor uplift. This number relates to the amplitude, spatial, and temporal distribution of the uplift. Tsunami trains (5a) are dominated by wavenumbers in the span where $F(\mathbf{k})$ is greatest.

The peak of F(k) corresponds to the characteristic dimension of the uplift. Large-dimensioned uplifts produce longer wavelength, hence lower frequency tsunami than small-dimensioned sources.

b) The 1/ cosh(kh) term low-pass filters the source spectrum F(**k**). Because $1/\cosh(kh) \rightarrow 1$ when $kh \rightarrow 0$, and $1/\cosh(kh) \rightarrow 0$ when $kh \rightarrow \infty$, the filter favors long waves. The form of the filter comes about from variation of the vertical eigenfunction $u_z(\omega,z)$ (equation 4) across the ocean layer. Because of the low-pass filter effect of the ocean layer, only wavelengths of the uplift source that exceed three times the ocean depth (i.e. $kh=2\pi h/\lambda < \approx 2$) contribute much to tsunamis.

c) The exponential term in (5a) contains all of the propagation information including travel time, ***geometrical spreading,*** and frequency dispersion (see below).

By rearranging equations (5a,b), vertical tsunami motions at **r** can also be written as

$$u_z^{surf}(\mathbf{r},t) = \mathrm{Re}\int_0^\infty \frac{k\,dk\, e^{-i\omega(k)t}}{2\pi\cosh(kh)} \sum_{n=-\infty}^{\infty} J_n(kr) e^{in\theta} F_n(k)$$

with

$$F_n(k) = \int_{\mathbf{r}_0} d\mathbf{r}_0\; u_z^{bot}(\mathbf{r}_0)\, J_n(kr_0)\, e^{i(\omega(k)\tau(\mathbf{r}_0) - n\theta_0)} \qquad (6)$$

Here θ marks conventional azimuth from north (the $\hat{\mathbf{x}}$ direction) of the observation point **r** from the co-ordinate origin. The $J_n(x)$ are cylindrical Bessel functions. For simply distributed uplift sources, (6) might be easier to evaluate than (5). For instance, if $\tau(\mathbf{r}_0)=0$ and the uplift is radially symmetric, then all of the terms in the sum save $F_0(k)$ vanish, and the tsunami is

$$u_z^{surf}(\mathbf{r},t) = \int_0^\infty \frac{k\,dk\cos[\omega(k)t]}{2\pi\cosh(kh)} J_0(kr) F_0(k) \qquad (7)$$

Magnitude M_w	Moment M_0 (Nm)	Area A (km^2)	Length L (km)	Width W (km)	Slip Δu (m)
6.5	6.3×10^{18}	224	28	8	0.56
7.0	3.5×10^{19}	708	50	14	1.00
7.5	2.0×10^{20}	2,239	89	25	1.78
8.0	1.1×10^{21}	7,079	158	45	3.17
8.5	6.3×10^{21}	22,387	282	79	5.66
9.0	3.5×10^{22}	70,794	501	141	10.0
9.5	2.0×10^{23}	223,872	891	251	17.8

Table 1. Relationship between earthquake magnitude and moment with values of fault area, length and mean slip for typical tsunami-generating earthquakes. This paper assumes $\log(L)=0.5M_w-1.8$, $\Delta u = 2\times10^{-5}L$, and $\lambda=\mu=5\times10^{10}$ Pa

A. Tsunami excitation by earthquakes

Earthquakes produce most tsunamis. Not surprisingly, earthquake parameters determine many of the characteristics of the sea waves. Earthquakes result from slip on faults and many parameters describe the process; three features however, are most important -- moment, mechanism and depth.

Moment measures earthquake strength. Moment M_o is the product of rigidity μ of the source region's rocks, fault area A, and average fault slip Δu. Earthquake moment and earthquake magnitude tie through a number of empirical formulae. One formula defines moment magnitude M_w as $M_w=(2/3)(\log M_o-9.05)$. Earthquake moment varies by 2×10^4 within the magnitude range

$6.5 \le M_w \le 9.5$ (Table 1). Even without a detailed understanding of tsunami generation, it is safe to suppose that the larger the earthquake moment, the larger the tsunami, all else fixed.

Mechanism specifies the orientation of the earthquake fault and the direction of slip on it. Usually, faults are idealized as plane rectangles with normal $\hat{\mathbf{n}}$. Three angles then, summarize earthquake mechanisms -- the strike and dip of the fault and the angle of slip vector $\hat{\mathbf{a}}$ measured from the horizontal in the plane of the fault. (Seismologists call this angle the "rake".) The role of fault mechanism on tsunami production is not as obvious as the influence of moment; however, one might suspect that earthquakes that affect large vertical displacements of the seafloor would be more effective than faults that make large horizontal displacements.

Earthquake *depth* needs no explanation. Because seafloor shifts cause tsunamis, the distance of the fault from the seafloor should be important. Presumably, deep earthquakes would produce less potent tsunamis than similar shallow earthquakes.

Numerical, or synthetic, tsunami waveforms quantify the roles of earthquake parameters on tsunami generation. For illustration, insert into (6) the surface uplift pattern $u_z^{bot}(\mathbf{r}_0)$ of a small earthquake fault (point source really) placed at depth d in a halfspace. Further assume that the uplift occurs instantly with $\tau(\mathbf{r}_0)=0$. (Actually, real earthquakes uplift the seafloor over several, or several tens of seconds. This distinction is not a big issue because tsunami waves have periods of many hundreds of seconds. Uplifts taking a few dozen seconds to develop still look "instantaneous" to tsunamis). Equation (6) becomes

$$u_z^{surf}(\mathbf{r},t) = \int_0^\infty k\, dk \frac{\cos\omega(k)t}{2\pi \cosh(kh)} \left[A\Delta u \mathbf{M}_{ij} \varepsilon_{ij} \right] \quad (8)$$

where

$$\begin{aligned}
\varepsilon_{xx} &= -\frac{1}{4}\left(\frac{\mu}{\lambda+\mu}\right) - kd\left[J_0(kr) - J_2(kr)\cos 2\theta\right]e^{-kd} \\
\varepsilon_{yy} &= -\frac{1}{4}\left(\frac{\mu}{\lambda+\mu}\right) - kd\left[J_0(kr) + J_2(kr)\cos 2\theta\right]e^{-kd} \\
\varepsilon_{xy} &= \varepsilon_{yx} = \frac{1}{4}\left(\frac{\mu}{\lambda+\mu}\right) - kd\left[J_2(kr)\sin 2\theta\right]e^{-kd} \\
\varepsilon_{zz} &= -\frac{1}{2}\left(\frac{\mu}{\lambda+\mu}\right) + kd\left[J_0(kr)\right]e^{-kd} \\
\varepsilon_{xz} &= \varepsilon_{xz} = \frac{kd}{2}\left[J_1(kr)\cos\theta\right]e^{-kd} \qquad (9) \\
\varepsilon_{yz} &= \varepsilon_{zy} = \frac{kd}{2}\left[J_1(kr)\sin\theta\right]e^{-kd}
\end{aligned}$$

The six elements of symmetric tensor

$$M_{jk} = (\hat{\mathbf{a}}_j\, \hat{\mathbf{n}}_k + \hat{\mathbf{n}}_j \hat{\mathbf{a}}_k) \quad (10)$$

capsulize the mechanism of the earthquake. In (10), $\hat{\mathbf{n}}$, $\hat{\mathbf{a}}$ are the fault normal and slip vector introduced above. A pure dip slip earthquake on a vertical north-south trending fault for instance, has $\hat{\mathbf{n}}=\hat{\mathbf{y}}$ and $\hat{\mathbf{a}}=\hat{\mathbf{z}}$, so $M_{yz}=M_{zy}=1$ and $M_{xx}=M_{yy}=M_{zz}=M_{xz}=M_{zx}=M_{xy}=M_{yx}=0$.

The bracketed terms in (8) contain all of the relationships between earthquake parameters and tsunami features. Some relationships are easy to spot: tsunami amplitudes from earthquakes are proportional to the product of fault area and average slip ($A\Delta u$); tsunami amplitudes decrease

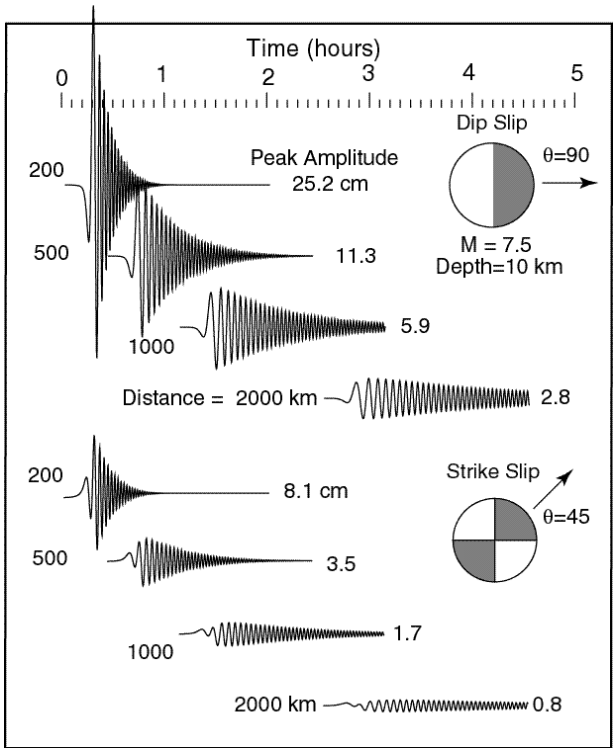

Figure 3. Synthetic record sections of vertical tsunami motions at distances of 200, 500, 1000 and 2000km from point dip slip (*top*) and strike slip (*bottom*) earthquakes of magnitude M_w=7.5 and depth 10 km. Time runs for five hours and the peak amplitude of each trace is given in cm at the right. The lower half of the focal sphere and azimuth of observation θ are shown toward the right. For other directions, the waveforms should be scaled by $\sin\theta$ and $\sin 2\theta$ respectively.

with earthquake depth via the e^{-kd} terms. The ε_{ij} provide the dependence of tsunami amplitude and azimuthal radiation pattern on source type. Equation (9) says that tsunamis from point sources radiate in azimuthal patterns no more intricate than $\sin 2\theta$ or $\cos 2\theta$.

Fig. 3 shows five hours of tsunami waveforms calculated from (8) at distances of r=200, 500, 1000, 2000km from dip slip (M_{yz}=M_{zy}=1) and strike slip (M_{xy}=M_{yx}=1) point sources of magnitude M_w=7.5 (ΔuA= $3.98\text{x}10^6\text{m}^3$. See Table 1) buried at 10 km depth. Sea waves from these sources have radiation patterns of $\sin\theta$ and $\sin 2\theta$ respectively. I compute the waveforms in Fig. 3 at the azimuth of maximum strength, $\theta=90^0$ and $\theta=45^0$. Frequency dispersion, with the long periods arriving first, is the most conspicuous feature of the waveforms. Tsunamis onset rapidly. They reach maximum height in the first few cycles and then decay slowly over an hour or more. Even for this large earthquake, tsunamis beyond 500km distance reach just a few cm --hardly killer waves. Note that if the observation direction was west versus east (Fig. 3 top), or northwest versus northeast (Fig. 3 bottom), the tsunami waveforms would be inverted. Whether tsunamis onset in a withdrawal or an inundation

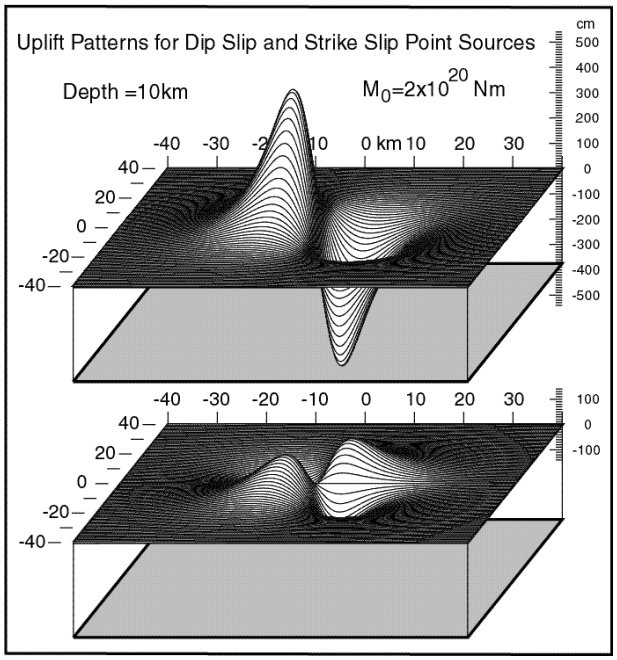

Figure 4. Static vertical displacements of the seafloor for the dip slip (*top*) and strike slip (*bottom*) earthquake point sources that generated the tsunamis of Fig. 3. Maximum excursions of the seafloor are 5.4 and 1.4 m respectively.

at a particular shoreline strictly depends on the style of faulting and the relative positions of the shore and the fault.

Fig. 3 demonstrates that for point sources, dip slip earthquakes produce 3 or 4 times larger tsunami than strike slip earthquakes of equal moment. The differences in generation efficiency are understood most easily by considering directly the seafloor deformation patterns $u_z^{bot}(\mathbf{r}_0)$. I find these patterns by setting t=0 and h=0 in (8) so $\cos\omega(k)t/\cosh(kh)=1$. Fig. 4 pictures the uplift patterns for the two faults of Fig. 3 where two ($\sin\theta$) and four-lobed ($\sin 2\theta$) deformations spread over a region 40km wide. The most striking contrast in the fields is maximum vertical displacement -- 1.4m for the strike slip versus 5.4m for the dip slip. It is no coincidence that the ratio of maximum uplift for these two faults replicates the ratio of tsunami heights in Fig 3. Afterall, vertical seafloor deformation drives tsunamis and vertical deformation is controlled largely by the rake of the slip vector $\hat{\mathbf{a}}$. Strike slip faults have a rake of 0^0. Dip slip faults have rake equal $\pm 90^0$. Further simulations show that, excepting very shallow, nearly horizontal faults, dip is not a terribly significant factor in tsunami production.

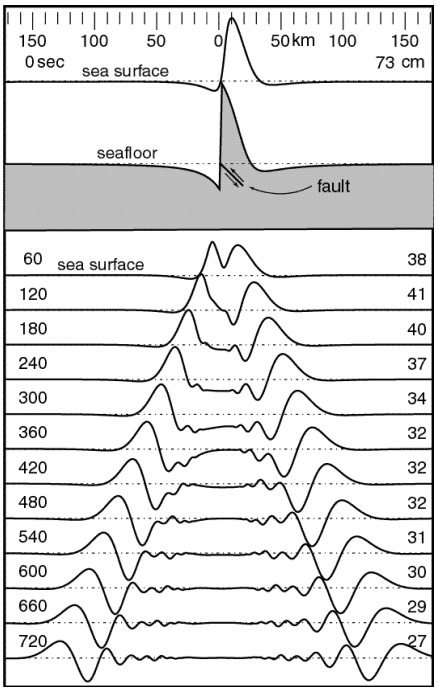

Figure 5a. Cross sections of expanding tsunami rings from a M7.5 thrust earthquake. The fault strikes north-south (into the page) and the sections are taken east-west. Elapsed time in seconds and maximum amplitude in cm are given at the left and right sides.

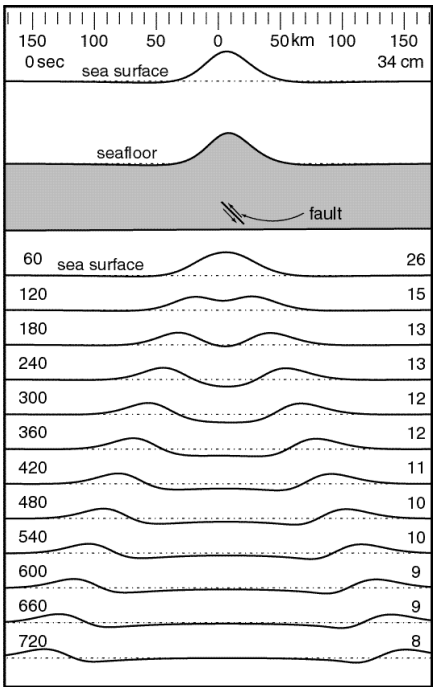

Figure 5b. Cross sections of expanding tsunami rings from the M7.5 thrust earthquake of Fig 5a, now buried 30 km. Deeper earthquakes make smaller and longer wavelength tsunamis.

The sea surface cross-sections in Figs. 5a and 5b chronicle the birth and early life of a sea wave spawned by M7.5 thrust earthquakes on 45^0 dipping planes. In these figures, I replace the idealized point sources of Figs. 3 and 4 with faults of typical dimension (L= 89km, W=25km and Δu= 1.78m. See Table 1). In Fig. 5a, the fault reaches to the sea floor. In Fig. 5b, the fault stops 30km down. Soon after earthquake, the sea surface forms “dimples” similar to those on the deformed the sea floor. The sea surface dimples however, are smoother and a bit lower

in amplitude because of the 1/cosh(kh) low pass filtering effect of the ocean layer. After a time roughly equal to the dimension of the uplift divided by tsunami speed $\sqrt{gh}$, the leading edges of the wave organize and begin to propagate outward as expanding rings. Early on, the wave appears as a single pulse. Characteristic tsunami dispersion begins to be seen only after 10 or 20 minutes. Consequently, for shorelines close to tsunami sources, seismic sea waves arrive mostly as a single pulse. For distant shorelines, sea waves arrive with many oscillations, dispersion having spread out the initial pulse.

The e^{-kd} terms in the tsunami excitation functions (9), let shallow earthquakes excite higher frequency tsunamis than deep earthquakes. (compare Fig. 5a with Fig. 5b). Higher frequency waves travel more slowly than longer period waves however, so high frequency waves contribute to peak tsunami height only while the tsunami propagates as a single pulse. After a few hundred kilometers of travel, high frequency waves drift to the back of the wave train (see Figure 5a) and no longer add to the tsunami maximum. At 200km distance, the shallow earthquake generates a wave about 3 times larger than the 30km deep event. If you were to track the waves out to 2000km however, you would find that the extra high frequencies in the shallow event will have fallen behind and that the maximum wave heights for the two events would be nearly equal. Beyond 2000km distance, any earthquake depth less than 30 km appears to be equally efficient in tsunamigenesis.

Faults of finite size, like those in Fig. 5, radiate tsunamis in distributions more complex than the

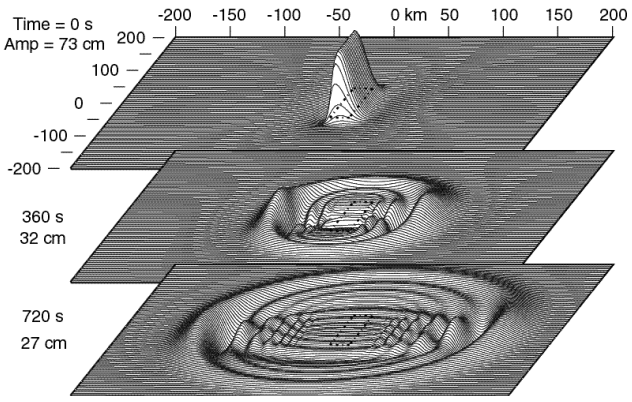

Figure 6. Views of the expanding tsunami rings from the earthquake in Fig. 5a at t= 360 and 720s. The dashed rectangle in the center traces the surface projection of the fault. For large earthquakes, nearly all tsunami energy beams perpendicular to the strike of the fault (*toward the left and right in this picture*).

$\sin\theta$ and $\sin 2\theta$ patterns from point sources. The largest earthquakes have fault lengths of several hundred kilometers. Simulations show that long earthquake faults, preferentially emit tsunamis in a tight beam perpendicular to the fault strike, regardless of the focal mechanism (see Fig. 6). Tsunamis radiated parallel to strike tend to be eliminated. This preferential beaming might simplify tsunami forecasting because it tells us which direction to look for the biggest waves. Although long faults focus waves at right angles to their length, the maximum amplitude of the waves do not exceed those expected from a point source of the same moment, mechanism and mean depth.

Maximum Tsunami Amplitude

One might boil-down tsunami hazard to a single question: What is the largest tsunami expected at distance r from an earthquake of magnitude M? A good question yes, but deciding what constitutes a “maximum tsunami” is not cut-and-dry. I

model them by using the most efficient focal mechanism (thrusting on 45° dipping fault that reaches to the sea floor) and observe them in the direction of maximum radiated strength (perpendicular to the strike of the fault. The cross sections of Fig. 5a duplicate these circumstances. The maximum tsunami calculation also supposes uniform moment release on typical-sized planer faults with lengths and widths taken from Table 1. (Be aware that a principal concern in tsunami forecasting are "anomalous earthquakes" -- those whose mean slip, fault size, or shape, don't match well with Table 1, or those with highly non-uniform slip distributions.) The bottom bound of the shaded areas in the Fig. 7 traces maximum open-ocean tsunami height from typical earthquakes in the magnitude range 6.5, to 9.5. The shaded areas include a factor-of-two excess, and probably give a good representation of peak open-ocean tsunami height $A_{max}^{ocean}(M,r)$ including most anomalous earthquakes.

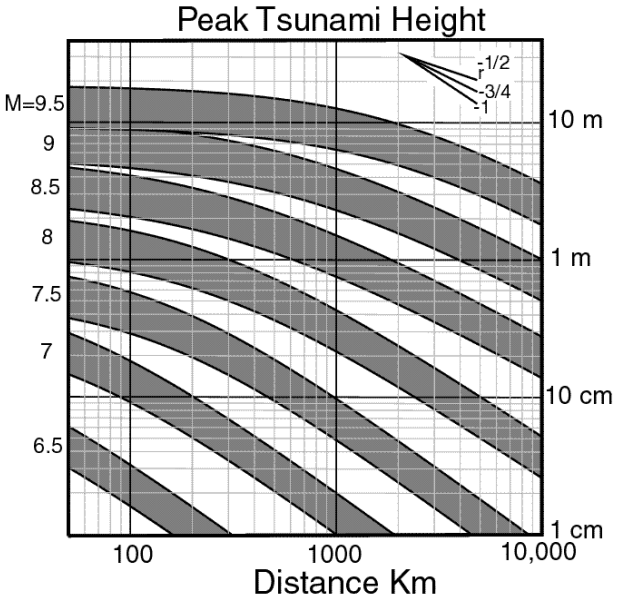

Figure 7. Computed maximum open-ocean tsunami height $A_{max}^{ocean}(M,r)$ versus distance from earthquakes of magnitude 6.5 to 9.5. The gray areas include an allowance for anomalous events. Ocean depth is 4000m. These curves do not include shoaling amplification factor S_L.

In the open-ocean, maximum tsunami heights vary from a few cm to 10-15m as M_w grows from 6.5 to 9.5. Compare the near-source amplitudes in Fig. 7 with the corresponding Δu in Table 1. As a rule of thumb, maximum tsunami amplitude in the open ocean can not be much greater than the earthquake's mean slip. This rule makes sense because the generated waves can not be much bigger than the amplitude of the seafloor uplift, and the seafloor uplift can not be much greater than the mean slip on the fault. Actually, earthquakes of magnitude less than M7.5 even have trouble making tsunamis as large as Δu. Their small faults can only deform an area of the same dimension as the ocean depth, so the 1/cosh(kh) low pass ocean filter takes a toll.

Fig. 7 shows that far from the large earthquakes, tsunami waves drop in amplitude with distance roughly like $r^{-.3/4}$; that is, if you double the distance the wave travels, the amplitude shrinks by $2^{-3/4}$=0.6. The amplitude decay rate is the product of two terms: a $r^{-1/2}$ factor that stems from geometrical spreading of the waves in ever-growing rings, and a factor $r^{-\chi}$ due to frequency dispersion that pulls apart of once pulse-like waves. The dispersion decay factor χ falls between 1/8 to 1/2 depending on the frequency content of the tsunami. Spatially larger (or deeper) deformation sources produce longer waves that are less affected by dispersion, so waves from them decay more slowly with distance. You can see the in-

fluence of the variable decay factor χ in Fig. 7 where the curves slope less for larger magnitude quakes.

The "attenuation curves" of Fig. 7 relate maximum tsunami amplitude to earthquake magnitude and earthquake distance. If one could estimate the frequency of occurrence of all magnitude earthquakes at a fixed ocean location, then the attenuation curves could be used to derive the heights and frequency of occurrence of tsunamis from that location anywhere else. This connection forms the first step in probabilistic tsunami hazard analysis (see Section VI).

B. Tsunami excitation from submarine landslides

Earthquakes parent most tsunamis, but other things do too. For instance, earthquake shaking often triggers landslides. If the slide happens under the sea, then tsunamis may form. Consider a seafloor landslide confined in a rectangle of length L and width W. To simulate the progression of a landslide disturbance, let a constant uplift u_0 start along one width of the rectangle and run down its length ($\hat{\mathbf{x}}$ direction, say) at velocity v_r, i.e. $\tau(\mathbf{r}_0)=x/v_r$ (see Fig. 8). Placing this $u_z^{bot}(\mathbf{r}_0)$ and $\tau(\mathbf{r}_0)$ into (5), I find tsunamis from this landslide source at observation point $\mathbf{r}$ and time t to be

$$u_z^{surf}(\mathbf{r},t) = \frac{u_0 LW}{4\pi^2} \mathrm{Re}\int_{\mathbf{k}} d\mathbf{k} \frac{e^{i(\mathbf{k}\cdot\mathbf{r}-\omega(k)t)} e^{-iX(\mathbf{k})}}{\cosh(kh)} \frac{\sin X(\mathbf{k})}{X(\mathbf{k})} \frac{\sin Y(\mathbf{k})}{Y(\mathbf{k})} \quad (11)$$

where

$$X(\mathbf{k}) = \frac{kL}{2}\left(\hat{\mathbf{k}}\cdot\hat{\mathbf{x}} - c(k)/v_r\right) \quad \text{and}$$

$$Y(\mathbf{k}) = \frac{kW}{2}\left(\hat{\mathbf{k}}\cdot\hat{\mathbf{y}}\right)$$

The $X(\mathbf{k})$ and $Y(\mathbf{k})$ factors, because they depend on the relative positions of the observation point and the landslide source, instill radiation patterns to the tsunami much like the ε_{ij} do for earthquakes. Fig. 8 pictures the tsunami computed from (11) for a 50 x 50km seafloor patch that is progressively uplifted by 1m due to a landslide. As cartooned, the uplift starts along the left edge of the slip zone and moves to the right. The figure snapshots the situation 357s after the slide started. Experiments like these reveal that, depending on the aspect ratio of the landslide and the ratio of slide velocity to the tsunami phase velocity, significant beaming and amplification of the tsunami are possi-

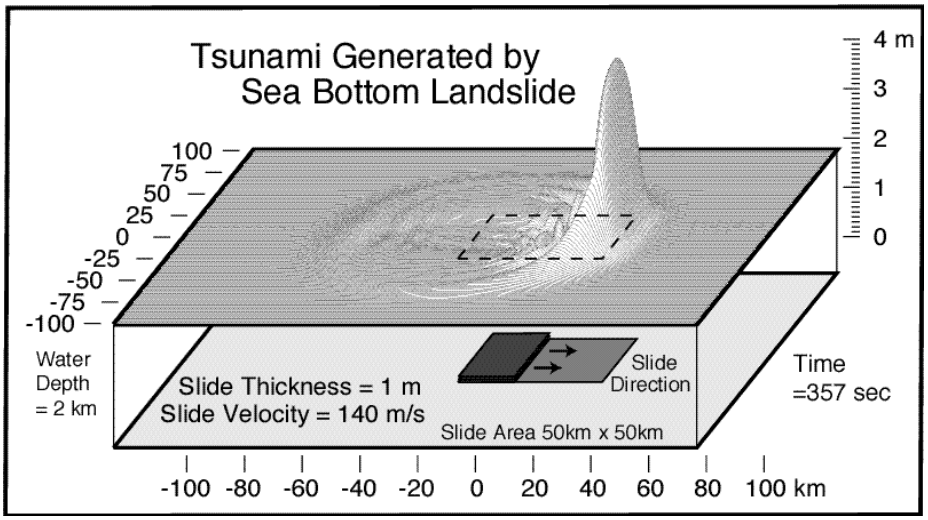

Figure 8. Tsunami produced by a submarine landslide. The slide is 1-m thick and occurs over a 50km by 50km area. The slide starts to the left and moves to the right at 140 m/s. Note the strong amplification of the wave in the slide direction.

ble. In particular, when the slide velocity v_r approaches the tsunami speed $c(k) \approx \sqrt{gh}$, then $X(\mathbf{k})$ is nearly zero for waves travelling in the slide direction. For observation points in this direction, the waves from different parts of the source arrive nearly "in phase" and constructively build. Fig. 8 highlights the beaming and amplification effects by evaluating (11) in a 2km-deep ocean and $v_r = \sqrt{gh}$ =134m/s. Witness the large tsunami pulse sent off in the direction of the slide. The tsunami peak stands more than three times the thickness of the slide. Fig. 8 pictures an extreme example; still, submarine landslides are prime suspects in the creation of "surprise tsunamis" from small or distant quakes. Surprise landslide tsunami might initiate well outside of the earthquake uplift area, or be far larger than expected from standard attenuation curves (Fig. 7).

C. Tsunami excitation from impacts

The sections above discussed tsunamis from earthquakes and landslides. One other class of tsunamis holds interest – those generated from impacts of comets and asteroids. To investigate impact tsunami, imagine that the initial stage of cratering by moderate size impactors excavates a radially symmetric, parabolic cavity of depth D_C and radius R_C

$$u_z^{impact}(\mathbf{r}) = D_C\,(1 - r^2/R_C^2) \qquad r \le \sqrt{2}\,R_C$$

$$u_z^{impact}(\mathbf{r}) = 0 \qquad r > \sqrt{2}\,R_C$$

Based on equation (5), the impact tsunami at observation point **r** and time t is

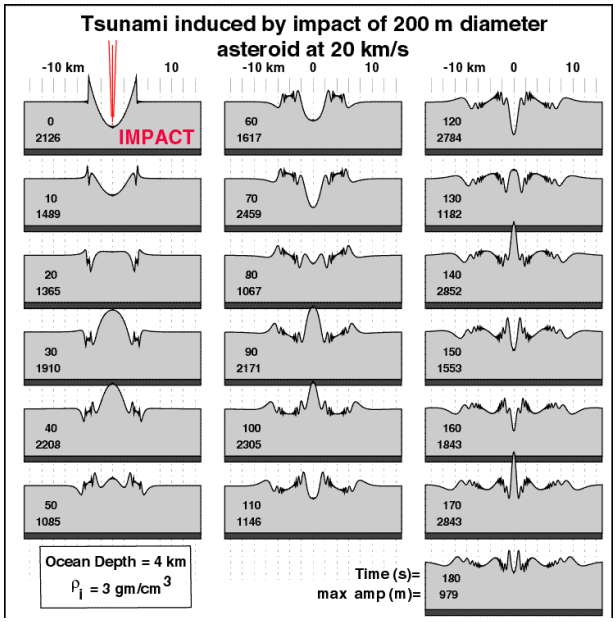

Figure 9. Computed tsunami induced by the impact of a 200m diameter asteroid at 20km/s. The waveforms (shown at 10s intervals) trace the surface of the ocean over a 30km cross section that cuts rings of tsunami waves expanding from the impact site at x=0. Maximum amplitude in meters is listed to the left.

$$u_z^{surf}(\mathbf{r},t) = \int_0^\infty \frac{k\,dk}{2\pi} \cos[\omega(k)t] J_0(kr) F_0(k) \qquad (12)$$

where

$$F_0(k) = \int_{\mathbf{r}_0} r\,d\mathbf{r}_0\; u_z^{impact}(\mathbf{r}_0)\, J_0(kr_0)$$

$$= \frac{8\pi D_c}{k^2}\left[J_2(k\sqrt{2}R_C) - kR_C J_1(k\sqrt{2}R_C)/\,2\sqrt{2}\right]$$

The principal distinction between (5) and (12) is the absence in the latter of the 1/cosh(kh) low pass ocean filter. Asteroids crater the surface of the ocean not the sea floor, so this filter does not come into play. If the depth of impact cavities equal 1/3 their diameter $d_c = 2R_C$, then D_c relates simply to the density, velocity and radius of the impacting body as

$$D_C = d_c/3 = (8\varepsilon\rho_I V_I^2/9\rho_w g)^{1/4} R_I^{3/4} \qquad (13)$$

In (13) ε is the fraction of the kinetic energy of impactor that goes into the tsunami wave. Impact experiments suggest ε≈0.15. With ρ_I=3gm/cm^3, ρ_w=1gm/cm^3 and V_I =20km/s, (13) returns crater depths of 1195, 2010, and 4000m for asteroids of radius R_I = 50, 100, and 250m.

Fig. 9 plots cross-sections of expanding rings of tsunami waves induced by the impact of a 200m diameter asteroid at 20km/s as computed by equation (12). Within 100km of ground zero, tsunamis from moderate size (100-250m) asteroids have heights of many 100s of meters and dwarf the largest (10-15m) waves parented by earthquakes. Fortunately, two features mitigate impact tsunami hazard: 1) Impact tsunamis have shorter wavelength than earthquake tsunamis so they decay faster with distance (more like r^{-1} versus $r^{-3/4}$ for earthquake tsunami). At 1000 and 3000 km, the tsunami in Fig. 9 would decay to 6 and 2m amplitude – still a concern, but not catastrophic. 2) Asteroids with diameters >200m impact Earth maybe every 2500 years, far less frequently than great M9 earthquakes that strike the planet about once in 25 years.

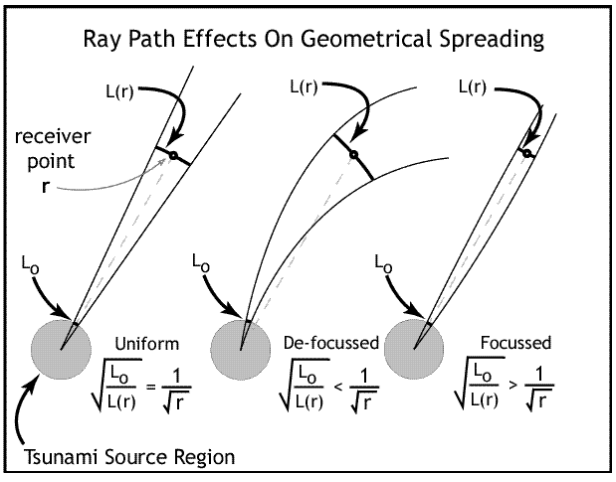

Figure 10. Effects of tsunami propagation path on geometrical spreading losses. Compared to a uniform ocean, focussed rays make for larger tsunami and de-focussed rays make for smaller ones.

IV. Tsunami Propagation

In uniform depth oceans, tsunamis propagate out from their source in circular rings (e.g. Fig. 6) with ray paths look like spokes on a wheel. In real oceans, tsunami speeds vary place to place (even at a fixed frequency). Tsunami ray paths refract and become bent. Consequently, in real oceans, both tsunami travel time and amplitude have to be adjusted relative to their values in uniform depth ones. To do this, it is best to transform the various integrals over wavenumber (e.g. 5, 6, 8, etc.) to integrals over frequency because wave frequency, not wave number, is conserved throughout. Using the relations u(ω)=dω/dk and c(ω)=ω/k(ω), I find that tsunami vertical motions from (12) for instance, are to a good approximation

$$u_z^{surf}(\mathbf{r},t) = \int_0^\infty \frac{\cos(\omega t)d\omega}{2\pi k(\omega)u(\omega)} J_0(\omega T(\mathbf{r},\omega))F_0(k(\omega)) \; G(\mathbf{r})S_L(\omega,\mathbf{r}) \quad (14)$$

In (14) the travel time of waves of frequency ω has been changed from r/c(ω) to

$$T(\mathbf{r},\omega) = \int_{raypath} d\, r / c(\omega,h(\mathbf{r})) \quad (15)$$

where the integral path traces the tsunami ray from the source to the observation point. Equa-

tion (14) also incorporates new geometrical spreading G(**r**), and shoaling factors $S_L(\omega,\mathbf{r})$. In a flat, uniform ocean, $1/\sqrt{r}$ amplitude losses occur due to geometrical spreading. The new

$$G(\mathbf{r}) = \sqrt{\frac{rL_o}{L(\mathbf{r})}} \quad (16)$$

accounts for topographic refraction that makes wave amplitudes locally larger or smaller. Fig. 10 cartoons typical refraction cases and gives meaning to (16) as being the ratio of cross-sectional distances L_0 and L(**r**) between adjacent rays measured near the source and near the observation point. Refraction might amplify or attenuate tsunami height by 50% over flat-ocean results. However, because only a finite amount of wave energy exists to disperse, concentrating it at one site, by necessity, robs it from another. When viewed regionally, refraction effects average out.

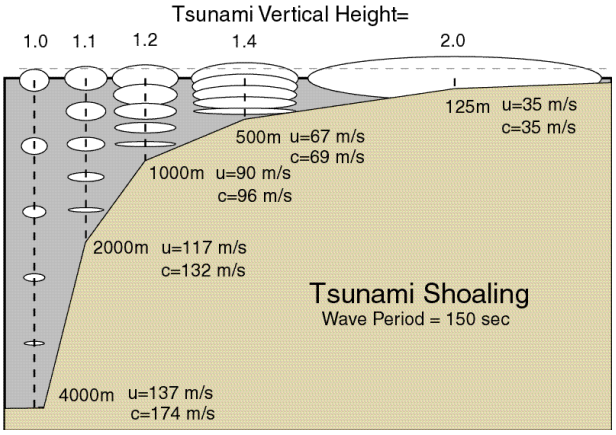

Figure 11. Effect of shoaling on tsunami eigenfunctions. The shallowing ocean near shore concentrates wave energy into smaller and smaller volumes. Tsunami amplitudes grow in response.

V. Tsunami Shoaling

Toward shore, real oceans shallow and the waves carried on them amplify. Often, the processes of wave amplification are lumped and labeled "run-up". Run-up has linear and non-linear elements. For the shoaling factor in (14), linear theory gives

$$S_L(\omega,\mathbf{r}) = \sqrt{\frac{u(\omega,h(\mathbf{r}))}{u(\omega,\ h_s)}} \quad (17)$$

Shoaling amplification depends on the ratio of group velocity at the nucleation-site and the coast-site (ocean depth h and h_s respectively). As does G(**r**), S_L naturally reverts to one in oceans of uniform depth. Fig. 11 shows the effect of shoaling on a tsunami wave of 150s period. Initially, a unit height wave begins to come ashore from 4000m of water at the left. As the water

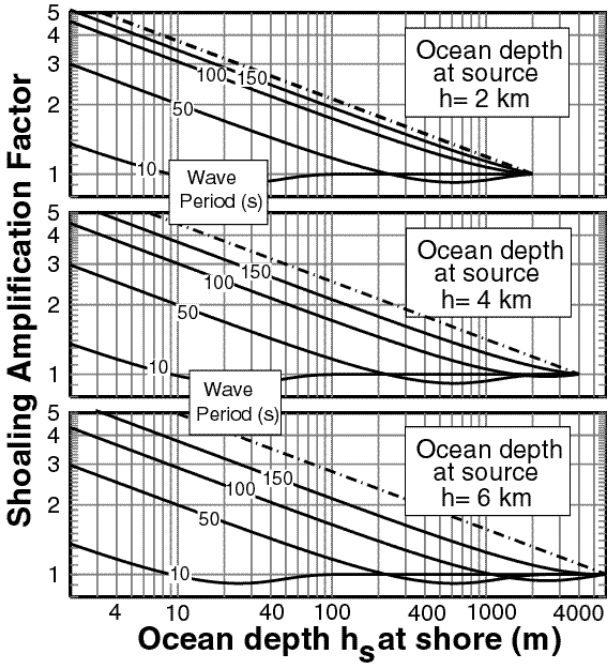

Figure 12. Shoaling amplification factor for ocean waves of various frequencies and source depths.

shallows, the velocity of the wave decreases and the waves grows in amplitude. By the time it reaches 125m depth it has slowed from 137m/s group velocity to 35m/s and grown in vertical height by a factor of two. As the wave comes closer to the beach it will continue to grow about a factor of two more -- then it will break. Fig. 12 plots (17) as a function of coast-site depth for sea wave periods from 10s, and ocean depths of 2, 4 and 6km. Beach waves at 10s period do not amplify much (perhaps 50%) in shoaling. Tsunami waves (100-2000s period) experience much stronger shoaling amplification -- about 3 to 6 over a wide range of conditions. For waves of period greater than 250s, (d_C>>h) $u(\omega,h)=(gh)^{1/2}$, $u(\omega,h_s)= (gh_s)^{1/2}$, and the shoaling factor reduces to Green's Law, $S_L=(h/h_s)^{1/4}$ (dashed line in Fig. 12.). Note that equation (17) depends on linear theory, so it can not take the wave all the way to shore where h_s vanishes. A safe bet sets $h_s=A_{crit}$, where A_{crit} is some tsunami height of concern – perhaps a few meters.

VI. Tsunami Hazard Estimation

How does one infer the statistical likelihood of a tsunami of a certain amplitude, striking a certain location, within a certain time interval? The procedure falls within the realm of probabilistic hazard estimation. I have already introduced a key element of the process -- the tsunami attenuation curves (Fig. 7) that provide $A_{max}^{ocean}(M,r)$, the maximum open ocean tsunami amplitude expected at a distance r from a magnitude M quake. Let $\mathbf{r}_S$ be a coastline point, $\mathbf{r}_0$ be a location of potential tsunami sources, and A_{crit} be a tsunami amplitude for which the probability of exceedence is desired. Using Green's Law for the shoaling factor, I need to solve

$$A_{crit} = A_{max}^{ocean}(M_C, |\mathbf{r}_S-\mathbf{r}_0|)\ (h(\mathbf{r}_s)/A_{crit})^{1/4}$$

for the minimum, or critical earthquake magnitude $M_C(r, A_{crit})$ such that the maximum tsunami height meets or exceeds A_{crit} at distance $|\mathbf{r}_S-\mathbf{r}_0|$. To be concrete, suppose that A_{crit}=2m, $|\mathbf{r}_S-\mathbf{r}_0|$=1000km, and the ocean depth at the source is $h(\mathbf{r}_s)$= 4000m. The shoaling factor comes to $(4000/2)^{1/4}$= 6.7, so an open ocean tsunami of 30cm will grow to 2m as it beaches. The attenuation curves in Fig. 7 indicate that to achieve a 30cm wave at 1000km distance, I need a M8 earthquake, i.e. M_C(1000km, 2m)=8. Any earthquake at distance r=1000km with magnitude greater than or equal to $M_C(r, A_{crit})$=8 could exceed the hazard threshold of A_{crit}=2m.

Now call n(M) the annual rate of earthquakes between magnitude M and M_I+dM_I per square meter of ocean near r_0. Seismologists supply n(M) mostly in the form of a Gutenberg-Richter relation, $n(M)=10^{a+bM}$. The annual rate of quakes that could exceed our threshold is

$$N(\mathbf{r}_s,\mathbf{r}_0,A_{crit}) = \int_{M_C(r,A_{crit})}^{M_{max}} n(M)dM \qquad (18)$$

$N^{-1}(\mathbf{r}_s,\mathbf{r}_0,A_{crit})$ is the mean recurrence interval of exceedence at coast-site $\mathbf{r}_s$ for the square meter of ocean at $\mathbf{r}_0$. To get the total rate for all tsunami sources under the ocean, integrate (18)

$$N(\mathbf{r}_s,A_{crit}) = \int_{\mathbf{r}_0(\mathbf{r}_s)} dA(\mathbf{r}_0)\ N(\mathbf{r}_s,\mathbf{r}_0,A_{crit}) \quad (19)$$

The domain of integration covers all ocean points $\mathbf{r}_0(\mathbf{r}_s)$ that are intervisible and unobstructed from $\mathbf{r}_s$. In time interval T, the Poissonian probability of one or more tsunami arriving at $\mathbf{r}_s$ that exceed A_{crit} in amplitude is

$$P(\mathbf{r}_s, T, A_{crit}) = 1 - e^{-N(\mathbf{r}_s, A_{crit})T} \quad (20)$$

Probability (20), being amplitude, location and time-interval specific, answers the question posed at the top of this section. Mapping $P(\mathbf{r}_s, T, A_{crit})$ along the coastlines of the world is work in progress.

VII. Tsunami Forecasting

Perhaps the ultimate goal of tsunami research is forecasting. Tsunami forecasts differ from tsunami hazard in that forecasting is case-specific, not statistical. A forecast predicts the strength of a particular tsunami given the knowledge that a potentially dangerous earthquake has occurred already. Tsunamis travel at the speed of a jet, but seismic waves that contain information about the earthquake faulting travel 20 or 30 times faster. For many places, there may be several hours between the arrivals of the seismic waves and the sea waves. This time could be spent analyzing seismograms, estimating earthquake parameters (namely location, moment, mechanism and depth), and forecasting the expected height of the oncoming wave with the aid of computer models of tsunami generation like those I have presented here. Reliable recovery of earthquake parameters from seismograms needs data from widely distributed stations. Likewise, forecasts are useful only if they can be issued before the arrival of the sea wave. It is well within current capabilities to record and to collect the needed seismic data anywhere in the world within the required time using modern digital seismometers and satellite/internet communication. When fed the seismic data, any number of sophisticated, and nearly automatic, computer programs already exist that could analyze and spit out the earthquake information quickly. So the prospects of tsunami forecasting are daunting, but realistic. Perhaps by the time of the next "killer tsunami", officials will be able to be definitive in their instructions to us to stay and play in the surf or to pick-up and leave the beach.

BIBLIOGRAPHY

Geist, E.L., 1998. Local Tsunamis and Earthquake Source Parameters, *Advances in Geophysics, 39*, 117-209.

Okal, E. A., 1988. Seismic Parameters Controlling Far-field tsunami amplitudes: A review, *Natural Hazards*, *1*, 67-96.

Ward, S. N., 1980. Relationships of tsunami generation and an earthquake source, *J. Phys. Earth, 28*, 441-474.

Ritsema, J., S. N. Ward and F. Gonzalez, 1995. Inversion of Deep-Ocean Tsunami Records for 1987-1988 Gulf of Alaska Earthquake Parameters, *Bull. Seism. Soc. Am., 85*, 747-754.

Ward, S. N. and E. Asphaug, 1999. Asteroid Impact Tsunami: A probabilistic hazard assessment, *Icarus*, submitted.